CMBES/SCGB
2025 CMBEC47/ACCES26
Fredericton, NB
May 27-29, 2025

End-To-End Automated Mean Linear Intercept Measurement System

Atallah Madi[1], Adrian D.C. Chan[1]

[1] Department of Systems and Computer Engineering, Carleton University, Ottawa, Canada

Abstract— **The Mean Linear Intercept (MLI) measurement is a quantitative metric for assessing air space size in histopathological images of lung tissue. Currently, MLI measurement involves human raters conducting manual image assessment that is time-consuming, labour-intensive, and subject to inter- and intra-rater variability. Our system utilizes a deep learning approach for semantic segmentation to achieve a fully automated MLI measurement system with a graphical user interface. The system was trained on mouse lung images and tested on a rat lung image to investigate the generalizability to other animal models. The system computed an MLI score of 62.20 within 90 minutes using 8255 field-of-view (FOV) images extracted from the whole slide image. The human rater found the MLI score to be 62.49 within 41 minutes using 500 randomly selected FOVs. This result suggests that the system maintains its accuracy with rat lung images. Although the system took twice as long as the human rater, it processed >16× more FOVs, which leads to lower standard error in the MLI score.**

Keywords— **mean linear intercept, histopathological images, semantic segmentation, automation, graphical user interface**

INTRODUCTION

The mean linear intercept (MLI) is a common quantitative metric in pulmonary morphometry that assesses air space size in histopathological lung images [1], [2]. MLI estimates the average chord length (L_m). It can be determined directly through measurements of the distances within an alveolus between the walls of the alveoli septa, or indirectly, through intersection counting. The MLI provides a measure of the mean free distance between gas exchange surfaces in the entire acinar air space.

MLI has been extensively applied in various clinical diagnostics and pathological research in pulmonary diseases. This includes mesenchymal stem cell therapy, a novel treatment for chronic obstructive pulmonary disease [3], analysis of emphysematous changes to lung parenchyma [4], and investigation of the effects of hyperoxia development [5]. In such studies, animal models are frequently used to mimic human chronic lung diseases and display the associated lung injury phenotype.

The indirect method is conducted by superimposing a horizontal guideline on a set of sub-images, called field-of-view images (FOVs), which are extracted from the lung whole slide image (WSI). If any part of the guideline intersects with the pleural space, bronchi, or blood vessels, that FOV is rejected. The remaining FOVs are accepted, and the number of intersections where the guideline fully crosses over an alveolar border wall is counted. The indirect MLI is calculated as:

$$MLI_{ind} = \frac{\sum_{i=1}^{N} G(i)}{\sum_{i=1}^{N} C(i)} \quad (1)$$

where N is the number of accepted FOV images, $G(i)$ is the length of the guideline superimposed on the i^{th} FOV image (in µm), and $C(i)$ is the number of intersection crossings for the i^{th} FOV image.

The direct method similarly rejects FOVs as the indirect method. The chord lengths along the horizontal guideline are measured in the accepted FOVs. The horizontal guideline is extended or truncated to avoid partial chords. The direct MLI is an unbiased estimate of L_m and is calculated as

$$MLI_{dir} = L_m = \frac{\sum_{i=1}^{N} \sum_{k=1}^{K(i)} L_i(k)}{\sum_{i=1}^{N} K(i)} \quad (2)$$

where N is the number of accepted FOV images, $K(i)$ is the number of chords measured in the i^{th} FOV image, and $L_i(k)$ is the length (in µm) of the k^{th} chord in the i^{th} FOV image.

The current MLI measurement system relies on the manual assessment of digital histopathological images through microscopic tools. In this process, a human rater visually examines the FOV images, rejecting or accepting them, and using the indirect approach, counts the number of intersections in accepted FOVs. The literature recommends using hundreds of accepted FOV images (at least 300 to 500) to evaluate MLI accurately [8],[9],[10]. It can take hours to complete the MLI measurement for a single WSI. While the direct method has its advantages, it would be more labour-intensive for a human to measure each chord length; hence, it is rarely used. The indirect method is still considered inefficient, time-consuming, and subject to inter- and intra-rater variability [10].

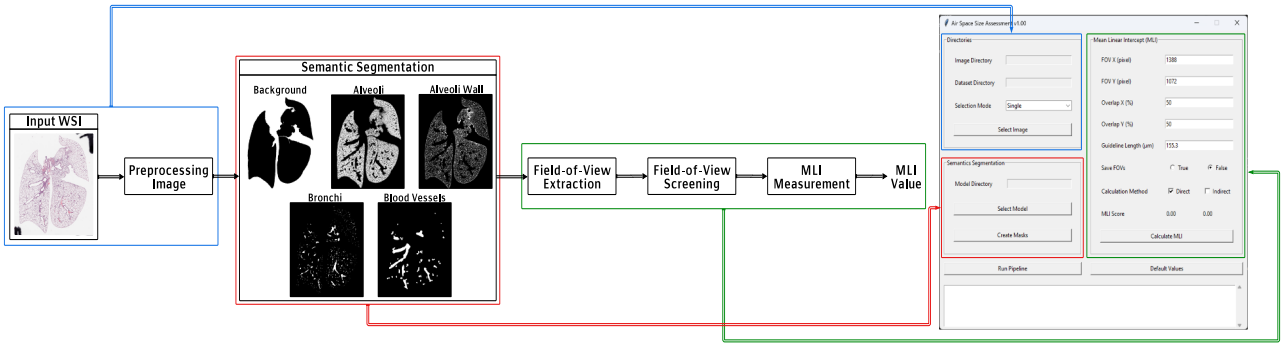

Figure 1: Block diagram of the modular automated system with the corresponding section in the interface.

We have developed an end-to-end automated MLI measurement system deployed in a graphical user interface (GUI). The system is modular with five main stages that are (Figure 1): 1) Image Preprocessing, 2) Semantic Segmentation, 3) Field-of-View Extraction, 4) Field-of-View Screening, and 5) MLI Measurement. This MLI measurement system is described in this paper. The system employs a deep learning approach for semantic segmentation, which was trained on mouse lung images, and was shown to be accurate with mean difference of 0.15 ± 1.96 when used for MLI scoring with mouse lung images [10],[11]. Since rat models are also common in lung research, in this study, we test the system on a rat WSI. While the basic lung structures are similar between mice and rats, rat lungs are larger, as are their alveoli [12]. Ideally, the system would remain accurate; otherwise, the system might require retraining of the deep learning segmentation model with rat WSIs, which would also require ground truth annotations.

METHODOLOGY

Image Preprocessing

In the image preprocessing step, colour normalization is applied using the colour mapping technique found in [13] to mitigate colour variation. Colour variations can be due to several factors, such as histochemical staining time and the quantity of used stain. Such variations can impact the segmentation performance and subsequently affect the calculation of the MLI score.

Semantic Segmentation

The goal of the Semantic Segmentation module is to segment lung biological structures into alveoli sacs, alveolar septa, blood vessels, bronchi, and pleural space. The high variability in the size and shape of these structures makes accurate segmentation challenging [14], [15]. We previously developed a two-stage multiresolution convolutional neural network (CNN) approach that allows for accurate segmentation of both small (e.g., alveoli) and large biological structures (e.g., bronchi) [16]. Because of the enormous size of WSIs (e.g., a single WSI can be 80,000×80,000 pixels in size), the WSI is tiled into small sub-images. In the first stage, four distinct CNNs are applied to input tiles at four different resolutions, extracting rich contextual information from each scale. The second stage aggregates the segmentation heatmaps from the four resolutions. In [16], this second stage applied a scaling factor to structures in the heatmaps, weighting the lower resolution heatmaps higher for larger structures, and lower for smaller structures. In the paper, we have simplified the aggregation by just averaging the different heatmaps (i.e., equal weighting); this simplification did not seem to have any significant impact on the segmentation accuracy.

The multiresolution CNN was trained on a dataset consisting of 20 histopathological WSIs of 20 mouse lungs, scanned at 20× resolution (0.5 µm per pixel). The dataset was provided by the Sinclair Centre for Regenerative Medicine at the Ottawa Hospital Research Institute in Ottawa, Ontario. The WSIs were prepared under all policies and protocols established by the University of Ottawa Animal Care Committee. Preparation methods for all the specimens are detailed in [10].

When a WSI is presented for segmentation, the multiresolution CNN outputs five binary segmentation masks, corresponding to the alveoli and its walls, blood vessels, bronchi, and pleural space.

Field-of-View Extraction

In the Field-of-View Extraction module, FOV images are extracted from the WSI, using a sliding window approach. The user can specify the FOV size and sliding window stride length. Default values are 1072 (height) × 1388 (width) pixels with 50% (536 pixels) and 50% (694 pixels) vertical and horizontal stride, respectively.

Field-of-View Screening

In the Field-of-View Screening module, a fixed horizontal guideline is superimposed on the center of each FOV image to be assessed for usability. If any part of the guideline intersects with any of the binary segmentation masks for pleural space, bronchi, or the blood vessels, then the FOV image is rejected; only the accepted FOV images are used in the MLI Measurement module. The user can specify the guideline length. The default value is 155.3 µm (312 pixels).

MLI Measurement

There are two methods to calculate the MLI: 1) indirect method, and 2) direct method, where the Alveoli Border Wall binary mask is used. In the indirect method, the system uses each accepted FOV image to count the number of times the alveoli septa fully cross the guideline and calculates the MLI using (1). In the direct method, the system measures the distance between consecutive alveolar septa along the guideline. To avoid partial chords, the guideline is extended if it falls within the alveolar air space. If the extension reaches the edge of the FOV image, it remains extended from the edge. The guideline is not extended if it falls within alveolar septa and extending it will result in rejecting the FOV image (i.e., it extends to the pleural space, a bronchus, or a blood vessel); instead, the guideline is truncated to the closest alveolar septa. After the guideline is appropriately adjusted, each chord along the guideline is measured, and the MLI is calculated using (2).

Graphical User Interface

The graphical interface encapsulates all the modules into an intuitive and user-friendly interface that is built in Python for the entire system (Figure 1). It allows the user to run a single WSI or multiple WSIs found within a directory. The user must also select the path for the trained multiresolution CNN model that will be used to segment the necessary binary masks. The interface is designed to provide the user with the ability to adjust the various parameters for MLI measurement to accommodate various research settings. This includes the size specifications of FOV images, such as width, height, and stride length, the option to save accepted and rejected FOV images, and guideline length; this allows for verification and validation by a human rater. The user can also choose to use the default parameters. The interface updates the user on the current stage through the textbox by using a multithreading process. The MLI score is displayed in the interface and saved locally in a CSV file with details for each FOV (e.g., location and number of crossings).

MLI Scoring

We tested the MLI measurement system on 1 histopathology WSI of a rat lung, which was also provided by the Sinclair Centre for Regenerative Medicine. Default parameters were used (FOV image size of 1072 × 1388 pixels with 50% overlap in the horizontal and vertical direction, guideline length of 312 pixels (155.3 µm)). This resulted in 8255 FOV images being extracted. A subset of 500 FOV images were randomly selected for indirect MLI scoring by a human rater (author A.M.).

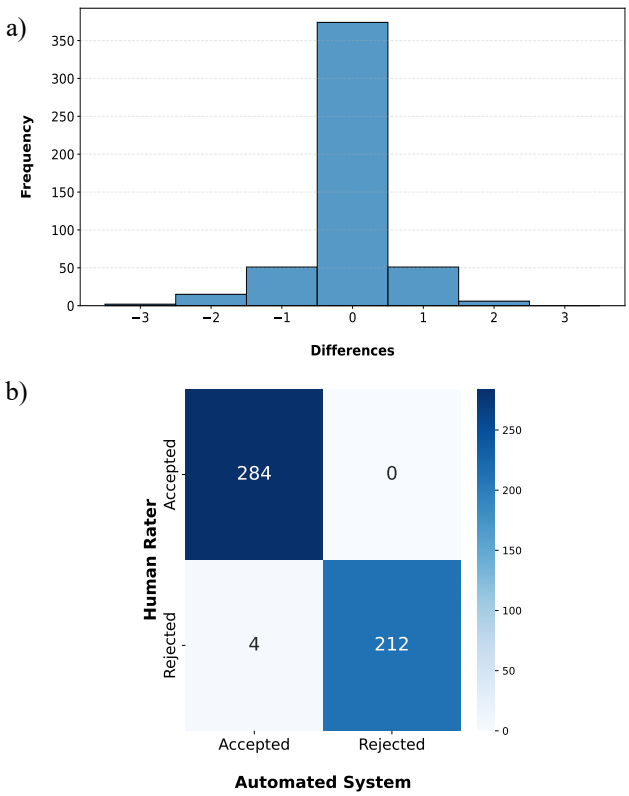

Figure 2: a) Histogram of differences in intersection crossing counts for accepted FOVs between the human rater and the system (Human Rater – System). b) Confusion matrix of the system for FOVs classification.

RESULTS AND DISCUSSION

When considering the FOV rejection accuracy, using the human rater as a ground truth, the system achieved a sensitivity and specificity of 100% and 98%, respectively. Figure 2b shows the confusion matrix for the extracted subset of 500 FOV images. The histogram plot (Figure 2a) shows the distribution of the differences between the human rater and the system counts for the number of intersections for FOVs that both the human rater and system accepted; the difference is positive if the system counted fewer intersections than the human rater. The human rater took 41 minutes to complete the MLI measurement using the indirect method on the 500 FOV images, reporting a MLI score of 62.49. The system generated the segmentation binary masks, evaluated the 8255 FOV images, and calculated the indirect MLI score of 62.20 within 90 minutes, on a PC, with an Intel Core 7 Processor v13 (up to 3.40 GHz) CPU, 32 GB of installed RAM, and a single NVIDIA GeForce RTX 3060 with 12 GB memory. The MLI scores differed by only 0.29 between the system and the human rater on the rat WSI utilizing a system that is trained on mice WSI. While the system took nearly twice as long as the human rater, it estimated the MLI using more than 16× the number of FOVs than the human rater. A larger number of FOVs, reduces the standard error, increasing the precision of the measurement. In addition, human raters are subject to inter- and intra-rater variability and would be unable to constantly process images, unlike a computer system. Finally, it should be noted that limited effort was made to optimize the system to minimize processing time.

CONCLUSION

The system demonstrated that, despite the segmentation model being trained on mice lung histopathology images, the model showed robust performance with a rat lung image, indicating that it is generalizable to other animal models. While the system took a longer time to compute MLI than the human rater, the main advantage is the ability to review a larger number of FOVs, which reduces the standard error, and the computer system can be used to process WSIs, continuously. Future work will include model optimization and increasing the efficiency of the system using model pruning and parallel prediction processes, respectively. The work presented in the paper is provided in a GitHub repository (e2emli).

ACKNOWLEDGEMENTS

This work was supported by the Natural Sciences and Engineering Research Council of Canada (NSERC) and clinical collaborators, Dr. Bernard Thébaud and Marissa Lithopoulos, from the University of Ottawa, Ottawa Hospital Research Institute, who provided the histopathology WSIs.

CONFLICT OF INTEREST

The authors declare that they have no conflict of interest.

REFERENCES

[1] M. S. Dunnill, "Quantitative methods in the study of pulmonary pathology," *Thorax*, vol. 17, no. 4, pp. 320–328, 1962.

[2] C. C. W. Hsia, D. M. Hyde, M. Ochs, E. R. Weibel, "An Official Research Policy Statement of the American Thoracic Society/European Respiratory Society: Standards for Quantitative Assessment of Lung Structure," Am J Respir Crit Care Med, vol. 181, issue. 4, pp. 394-418, Feb 2010.

[3] D. Weiss, R. Casburi, R. Flannery, M. LeRoux-Williams, D. P. Tashkin., "A placebo-controlled, randomized trial of mesenchymal stem cells in COPD," Chest, vol. 143, pp. 1590-1598, June 2013.

[4] W. Mitzner, "Use of mean airspace chord length to assess emphysema," J Appl Physiol., vol. 6, no. 105, pp. 1980-1981, Dec 2008

[5] M. Hurskainen et al., "Single cell transcriptomic analysis of murine lung development on hyperoxia-induced damage, " Nat Commun, vol. 1, no. 12, pp. 1565, Mar 2021.

[6] Q. Zhao, M. Meng, R. Kumar, Y. Wu, J. Huang, N. Lian, Y. Deng, S. Lin., "The impact of COPD and smoking history on the severity of COVID-19: A systemic review and meta-analysis, " J Med Virol, vol. 10, no. 92, pp. 1915-1921, Oct 2020.

[7] H. C. Chuang, Y. Y. Chen, T. C. Hsiao, H. C. Chou, H. P. Kuo, P. H. Feng et al., "Alteration in angiotensin-converting enzyme 2 by PM1 during the development of emphysema in rats, " ERJ Open Res, vol. 6, issue. 4, Oct 2020.

[8] Knudsen L, Weibel ER, Gundersen HJG, Weinstein F V., Ochs M. Assessment of air space size characteristics by intercept (chord) measurement: An accurate and efficient stereological approach. J Appl Physiol. 2010. doi:10.1152/japplphysiol.01100.2009

[9] G. Crowley, S. Kwon, E. J. Caraher, S. H. Haider, R. Lam, P. Batra, D. Melles, M. Liu, A. Nolan., "Quantitative lung morphology: semiautomated measurement of mean linear intercept," BMC Pulmonary Medicine, vol. 19, pp. 206-209, Nov 2019.

[10] S. Salsabili, M. Lithopoulos, S. Sreeraman, A. Vadivel, B. Thebaud, A. D. C. Chan, E. Ukwatta., "Fully automated estimation of the mean linear intercept in histopathology images of mouse lung tissue," J. of Medical imaging, vol. 8, March 2021.

[11] D. Politis, S. Salsabili and A. D. C. Chan, "An Automated Tool to Assess Air Space Size in Histopathology Images of Lung Tissue," 2022 IEEE International Instrumentation and Measurement Technology Conference (I2MTC), Ottawa, ON, Canada, 2022, pp. 1-6.

[12] Irvin, Charles G., and Jason HT Bates. "Measuring the lung function in the mouse: the challenge of size." Respiratory research 4 (2003): 1-9.

[13] E. Reinhard, M. Ashikhmin, B. Gooch, P. Shirley, "Color transfer between images," IEEE Comput Graph Appl, vol. 21, issue. 5, pp. 34-41, Oct 2001.

[14] M. Owais, N. R. Baek, K. R. Park, "DMDF-Net: Dual Multiscale Dilated Fusion Network for Accurate Segmentation of Lesions Related to COVID-19 in Lung Radiographic Scans", Expert Syst Appl, vol. 202, May 2022.

[15] X. Li, W. Li and R. Tao, "Staged Detection–Identification Framework for Cell Nuclei in Histopathology Images," IEEE Trans Instr Measur, vol. 69, issue. 1, pp. 183-193, Jan 2020.

[16] S. Salsabili, A. D. C. Chan, and E. Ukwatta, "Multiresolution semantic segmentation of biological structures in digital histopathology," J. Med. Imaging, vol. 11, pp. 037501-037501, 2024.